Hindawi Publishing Corporation
Journal of Combustion
Volume 2012, Article ID 794671, 17 pages
doi:10.1155/2012/794671

*Research Article*

# *A Priori* Assessment of Algebraic Flame Surface Density Models in the Context of Large Eddy Simulation for Nonunity Lewis Number Flames in the Thin Reaction Zones Regime

**Mohit Katragadda,[1] Nilanjan Chakraborty,[1] and R. S. Cant[2]**

[1] *School of Mechanical and Systems Engineering, Newcastle University, Claremont Road, Newcastle upon Tyne NE1 7RU, UK*
[2] *Engineering Department, Cambridge University, Trumpington Street, Cambridge CB2 1PZ, UK*

Correspondence should be addressed to Nilanjan Chakraborty, nilanjan.chakraborty@newcastle.ac.uk

Received 21 March 2012; Accepted 24 June 2012

Academic Editor: Andrei N. Lipatnikov



The performance of algebraic flame surface density (FSD) models has been assessed for flames with nonunity Lewis number (Le) in the thin reaction zones regime, using a direct numerical simulation (DNS) database of freely propagating turbulent premixed flames with Le ranging from 0.34 to 1.2. The focus is on algebraic FSD models based on a power-law approach, and the effects of Lewis number on the fractal dimension $D$ and inner cut-off scale $\eta_i$ have been studied in detail. It has been found that $D$ is strongly affected by Lewis number and increases significantly with decreasing Le. By contrast, $\eta_i$ remains close to the laminar flame thermal thickness for all values of Le considered here. A parameterisation of $D$ is proposed such that the effects of Lewis number are explicitly accounted for. The new parameterisation is used to propose a new algebraic model for FSD. The performance of the new model is assessed with respect to results for the generalised FSD obtained from explicitly LES-filtered DNS data. It has been found that the performance of the most existing models deteriorates with decreasing Lewis number, while the newly proposed model is found to perform as well or better than the most existing algebraic models for FSD.

## 1. Introduction

Reaction rate closure based on flame surface density (FSD) is one of the most popular approaches to combustion modelling in turbulent premixed flames [1–11]. In the context of LES the generalised FSD ($\Sigma_{\text{gen}}$) is defined as follows [3–11]:

$$\Sigma_{\text{gen}} = \overline{|\nabla c|}. \tag{1}$$

where the overbar denotes the LES filtering operation. The reaction progress variable $c$ may be defined in terms of a reactant mass fraction $Y_R$, for example, $c = (Y_{R0} - Y_R)/(Y_{R0} - Y_{R\infty})$ such that $c$ rises monotonically from zero in fresh reactants (subscript 0) to unity in fully burned products (subscript $\infty$).

In the context of LES, several models have been proposed for the wrinkling factor $\Xi$ [12–16], which is often used in the context of thickened flame modelling [13, 14]. The wrinkling factor $\Xi$ is closely related to $\Sigma_{\text{gen}}$ according to [12–16]:

$$\Xi = \frac{\Sigma_{\text{gen}}}{|\nabla \bar{c}|}. \tag{2a}$$

Often, $\Xi$ is expressed in terms of a power-law expression [7, 9, 13, 14] $\Xi = (\eta_0/\eta_i)^{D-2}$ in which $\eta_0$ and $\eta_i$ are the outer and inner cut-off scales and $D$ is the fractal dimension. This leads to a power-law expression for $\Sigma_{\text{gen}}$ as:

$$\Sigma_{\text{gen}} = \Xi |\nabla \bar{c}| = \left(\frac{\Delta}{\eta_i}\right)^{D-2} |\nabla \bar{c}|, \tag{2b}$$

where, for LES, the outer cut-off scale $\eta_o$ is taken to be equal to the filter width $\Delta$. According to Peters [17], $\eta_i$ scales with the Gibson length scale $L_G = S_L^3/\varepsilon$ in the corrugated flamelets (CF) regime, and with the Kolmogorov length scale $\eta = (\nu^3/\varepsilon)^{1/4}$ in the thin reaction zones (TRZ) regime. Here, $S_L$ is the unstrained laminar burning velocity, $\nu$ is the kinematic viscosity in the unburned gas, and $\varepsilon$ is the dissipation rate of turbulent kinetic energy. Experimental analyses by Knikker et al. [7] and Roberts et al. [18] indicated that $\eta_i$ scales with the Zel'dovich flame thickness $\delta_Z = \alpha_{T0}/S_L$, where $\alpha_{T0}$ is the thermal diffusivity in unburned gases. A recent *a priori* DNS analysis [9] demonstrated that $\eta_i$ scales with $L_G$ and $\eta$ for the CF and TRZ regimes, respectively, as suggested by Peters [17]. However, $\eta_i$ is also found to scale with thermal flame thickness $\delta_{\text{th}}$ in both the CF and TRZ regimes [9]. North and Santavicca [19] parameterised $D$ in terms of the root-mean-square (rms) turbulent velocity fluctuation $u'$ as: $D = 2.05/(u'/S_L + 1) + 2.35/(S_L/u' + 1)$, whereas Kerstein [20] suggested that $D$ increases from 2 to 7/3 for increasing values of $u'/S_L$, where $D = 7/3$ is associated with the material surface.

Since combustion is set to remain a major practical means of energy conversion for the foreseeable future, it has become necessary to find novel ways to reduce carbon emissions from relatively conventional combustion systems. One such approach is the use of hydrogen-blended hydrocarbon fuels in IC engines, aeroengines, and furnaces. Increased abundance of fast diffusing species such as H and $H_2$ leads to significant effects of differential diffusion of heat and mass in hydrogen-blended flames [21, 22], whereas these effects are relatively weaker in conventional hydrocarbon flames [22, 23]. The differential rates of thermal and mass diffusion in premixed flames are often characterised by the Lewis number Le which is defined as the ratio of the thermal diffusivity to mass diffusivity (i.e., $\text{Le} = \alpha_T/D_c$). Assigning a global characteristic value of Le is not straightforward since many species with different individual values of Le are involved in actual combustion. Often the Lewis number of the deficient reactant species is used as the characteristic Le [21, 24–28] and this approach has been adopted here. It is worth noting that, to date, most FSD-based modelling has been carried out for unity Lewis number flames (e.g., [1–11]) and the effects of differential diffusion of heat and mass on the statistical behaviour of FSD have rarely been addressed [28]. More specifically the effects of Le on $D$ and $\eta_i$ have not yet been analysed in detail, or in the context of power-law FSD reaction rate models. Moreover, most algebraic models for $\Sigma_{\text{gen}}$ have been proposed for the CF regime where the effects of Le are not accounted for. Thus, it is important to assess the performance of existing models for combustion in the TRZ regime with nonunity Lewis number.

The present study aims to bridge this gap in the existing literature. In this respect the main objectives of the work are as the following.

(i) To understand the effects of Lewis number on $D$ and $\eta_i$ in the context of LES modelling.

(ii) To assess the performance of existing wrinkling factor-based algebraic models of FSD in the context of LES for flames with nonunity global Lewis number based on *a priori* DNS analysis.

(iii) To identify or develop a power-law-based algebraic model for FSD in the context of LES which is capable of predicting the correct behaviour of FSD even for nonunity Lewis number flames.

The rest of the paper is organised as follows. An overview of the different algebraic FSD models considered here are presented in the next section. This will be followed by a brief discussion of the numerical implementation. Following this, results will be presented and subsequently discussed. Finally the main findings will be summarised and conclusions will be drawn.

## 2. Overview of Power-Law-Based FSD Models

A model for $\Xi$ suggested by Angelberger et al. [4] (FSDA model) can be written in terms of $\Sigma_{\text{gen}}$ as follows:

$$\Sigma_{\text{gen}} = \left[1 + a\Gamma\left(\frac{u'_\Delta}{S_L}\right)\right]|\nabla \bar{c}|, \tag{3a}$$

where $a = 1.0$ is a model parameter, $u'_\Delta = \sqrt{2\widetilde{k}_\Delta/3}$ is the subgrid turbulent velocity fluctuation, $\widetilde{k}_\Delta = (\widetilde{u_i u_i} - \widetilde{u}_i\widetilde{u}_i)/2$ is the subgrid turbulent kinetic energy and $\widetilde{Q} = \overline{\rho Q}/\bar{\rho}$ denotes the Favre-filtered value of a general quantity $Q$. In (3a), $\Gamma$ is an efficiency function which is given by:

$$\Gamma = 0.75\exp\left[-1.2\left(\frac{u'_\Delta}{S_L}\right)^{-0.3}\right]\cdot\left(\frac{\Delta}{\delta_z}\right)^{2/3} \tag{3b}$$

Weller et al. [12] also presented an algebraic model for $\Xi$, which can be recast in the form (FSDW model):

$$\Sigma_{\text{gen}} = [1 + 2\,\widetilde{c}(\Theta - 1)]|\nabla \bar{c}|, \tag{4}$$

where $\Theta = 1 + 0.62\sqrt{u'_\Delta/S_L}\,\text{Re}_\eta$ and $\text{Re}_\eta = u'_\Delta \cdot \eta/\nu$ with $\eta$ and $\rho_0$ denoting the Kolmogorov length scale and unburned gas density respectively. Colin et al. [13] proposed an algebraic model for $\Xi$, which can be expressed in terms of FSD (FSDC model) as:

$$\Sigma_{\text{gen}} = \left[1 + \alpha\,\Gamma\left(\frac{u'_\Delta}{S_L}\right)\right]|\nabla \bar{c}|, \tag{5}$$

where $\Gamma$ is given by (3b), $\alpha = \beta \times 2\ln(2)/[3c_{ms}(\text{Re}_t^{1/2} - 1)]$ with $\text{Re}_t = \rho_0 u' l/\mu_0$, where $\mu_0$ is the unburned gas viscosity and $l$ is the integral length scale, $\beta = 1.0$ and $c_{ms} = 0.28$. The FSDC model requires three input parameters, namely $u'_\Delta/S_L$, $\Delta/\delta_z$, and $\text{Re}_t$. Charlette et al. [14] reduced the input parameters to only $u'_\Delta/S_L$ and $\Delta/\delta_z$ by using (FSDCH model):

$$\Sigma_{\text{gen}} = \left(1 + \min\left[\frac{\Delta}{\delta_z}, \Gamma_\Delta\left(\frac{u'_\Delta}{S_L}\right)\right]\right)^{\beta_1}|\nabla \bar{c}|, \tag{6}$$

with the efficiency function

$$\Gamma_\Delta = \left[\left(\left(f_u^{-a_1} + f_\Delta^{-a_1}\right)^{-1/a_1}\right)^{-b_1} + f_{\text{Re}}^{-b_1}\right]^{-1/b_1}, \tag{7a}$$

Table 1

(a) Initial values of the simulation parameters and nondimensional numbers relevant to DNS database

| Case | Le | $u'/S_L$ | $l/\delta_{th}$ | $\tau$ | $Re_t$ | Da | Ka |
|---|---|---|---|---|---|---|---|
| A | 0.34 | 7.5 | 2.45 | 4.5 | 47.0 | 0.33 | 9.92 |
| B | 0.6 | 7.5 | 2.45 | 4.5 | 47.0 | 0.33 | 9.92 |
| C | 0.8 | 7.5 | 2.45 | 4.5 | 47.0 | 0.33 | 9.92 |
| D | 1.0 | 7.5 | 2.45 | 4.5 | 47.0 | 0.33 | 9.92 |
| E | 1.2 | 7.5 | 2.45 | 4.5 | 47.0 | 0.33 | 9.92 |

(b) List of initial simulation parameters and nondimensional numbers for the DNS database based on which the $Re_t$ dependence of $D$ is parameterised

| Case | $u'/S_L$ | $l/\delta_{th}$ | $\tau$ | $Re_t$ | Da | Ka |
|---|---|---|---|---|---|---|
| A1 | 5.0 | 1.67 | 4.5 | 22 | 0.33 | 6.54 |
| B1 | 6.25 | 1.44 | 4.5 | 23.5 | 0.23 | 9.84 |
| C1 | 7.5 | 2.5 | 4.5 | 49.0 | 0.33 | 9.84 |
| D1 | 9.0 | 4.31 | 4.5 | 100.0 | 0.48 | 9.84 |
| E1 | 11.25 | 3.75 | 4.5 | 110 | 0.33 | 14.73 |

where $Re_\Delta = u'_\Delta \Delta/\nu$ and with model constants $b_1 = 1.4$, $\beta_1 = 0.5$, $C_k = 1.5$, and functions $a_1$, $f_u$, $f_\Delta$, and $f_{Re}$ are defined by:

$$a_1 = 0.60 + 0.20\exp\left[-0.1\frac{u'_\Delta}{S_L}\right] - 0.20\exp\left[-0.01\frac{\Delta}{\delta_z}\right],$$

$$f_u = 4\left(\frac{27}{110}C_k\right)^{1/2}\left(\frac{18}{55}C_k\right)\left(\frac{u'_\Delta}{S_L}\right)^2,$$

$$f_\Delta = \left\{\left(\frac{27}{110}C_k\pi^{4/3}\right)\left[\left(\frac{\Delta}{\delta_z}\right)^{4/3} - 1\right]\right\}^{1/2},$$

$$f_{Re} = \left[\frac{9}{55}\exp(-1.5C_k\pi^{4/3}Re_\Delta^{-1})\right]^{1/2}Re_\Delta^{1/2}. \tag{7b}$$

Knikker et al. [7] proposed a model for $\Sigma_{gen}$ (FSDK model) as:

$$\Sigma_{gen} = \left(\frac{\Delta}{\eta_i}\right)^{\beta_k}|\nabla\bar{c}|, \tag{8}$$

where the inner cut-off scale $\eta_i$ is taken to be $\eta_i = 3\delta_z$ and $\beta_k$ is estimated based on a dynamic formulation as $\beta_k = [\log\langle|\nabla\bar{c}|\rangle - \log\langle|\nabla\hat{\bar{c}}|\rangle]/\log\gamma$, where $\hat{\bar{c}}$ denotes the reaction progress variable at the test filter level $\gamma\Delta$. Fureby [16] proposed a model for $\Xi$ which can be written in terms of $\Sigma_{gen}$ (FSDF model) as:

$$\Sigma_{gen} = \left[\Gamma\left(\frac{u'_\Delta}{S_L}\right)\right]^{D-2}\cdot|\nabla\bar{c}|, \tag{9}$$

where $\Gamma$ is given by (3b), and $D$ is specified according to the parameterisation $D = 2.05/(u'_\Delta/S_L + 1) + 2.35/(S_L/u'_\Delta + 1)$ [19].

In the present study, the performance of each algebraic model described above is assessed with respect to $\Sigma_{gen}$ obtained from DNS. There are three requirements for each model. Firstly, the volume-averaged value of $\Sigma_{gen}$ represents the total flame surface area, and therefore this quantity should not change with $\Delta$. Secondly, the model should be able to capture the correct variation of the averaged value of $\Sigma_{gen}$ conditional on $\bar{c}$ across the flame brush. Thirdly, the correlation coefficient between the modelled and actual values of $\Sigma_{gen}$ should be as close to unity as possible in order to capture the effects of local strain rate and curvature on $\Sigma_{gen}$.

## 3. Numerical Implementation

For the purposes of the analysis, a DNS database of three-dimensional turbulent premixed flames has been generated using the compressible DNS code SENGA [29]. Until recently most combustion DNS was carried out either in three dimensions with simplified chemistry or in two dimensions with detailed chemistry due to the limitations of available computational power. Although it is now possible to carry out three-dimensional DNS with detailed chemistry, such computations remain extremely expensive [30] and are not practical for a parametric study as in the present case. Thus three-dimensional DNS with single-step Arrhenius type chemistry has been used in the present study in which the effects of Lewis number are to be investigated in isolation.

For the present DNS database, the computational domain is considered to be a cube of size $24.1\delta_{th} \times 24.1\delta_{th} \times 24.1\delta_{th}$, which is discretised using a uniform grid of $230 \times 230 \times 230$. The grid spacing is determined by the flame resolution, and in all cases, about 10 grid points are kept within $\delta_{th} = (T_{ad} - T_0)/\max|\nabla\hat{T}|_L$, where $T_{ad}$, $T_0$ and $\hat{T}$ are the adiabatic flame, unburned reactant and instantaneous dimensional temperatures respectively, and the subscript $L$ is used to refer to unstrained planar laminar flame quantities. The boundaries in the direction of mean flame propagation are taken to be partially nonreflecting and are specified using the Navier Stokes Characteristic Boundary Conditions formulation [31], while boundaries in the transverse direction were taken to be periodic. A 10th order

central difference scheme was used for spatial discretisation for internal grid points and the order of differentiation gradually decreases to a one-sided second-order scheme at non-periodic boundaries [29]. A low storage 3rd-order Runge-Kutta scheme [32] is used for time advancement. The turbulent velocity field is initialised by using a standard pseudo-spectral method [33], and the flame is initialised using an unstrained planar steady laminar flame solution.

The initial values of $u'/S_L$ and $l/\delta_{\text{th}}$ for all the flames considered here are shown in Table 1 along with the values of heat release parameter $\tau = (T_{\text{ad}} - T_0)/T_0$, Damköhler number $\text{Da} = lS_L/u'\delta_{\text{th}}$, Karlovitz number $\text{Ka} = (u'/S_L)^{3/2}(lS_L/\alpha_{T0})^{-1/2}$ and turbulent Reynolds number $\text{Re}_t = \rho_0 u' l/\mu_0$. For all cases Ka remains greater than unity, which indicates that combustion is taking place in the TRZ regime [17]. Standard values are taken for Prandtl number ($\text{Pr} = 0.7$), ratio of specific heats ($\gamma_G = C_P/C_V = 1.4$), and the Zel'dovich number ($\beta_Z = T_{\text{ac}}(T_{\text{ad}} - T_0)/T_{\text{ad}}^2 = 6.0$), where $T_{\text{ac}}$ is the activation temperature.

In all cases, statistics were collected after three eddy turnover times (i.e., $3t_f = 3l/u'$), which corresponds to one chemical time scale (i.e., $t_c = \delta_{\text{th}}/S_L$). The turbulent kinetic energy and its dissipation rate in the unburned reactants ahead of the flame were slowly varying at $t_{\text{sim}} = 3.0\ l/u'$ and the qualitative nature of the statistics was found to have remained unchanged since $t = 2.0\ l/u'$ for all cases. By the time the statistics were extracted, the value of $u'/S_L$ in the unburned reactants ahead of the flame had decayed by about 50%, while the value of $l/\delta_{\text{th}}$ had increased by about 1.7 times, relative to their initial values. Further details on the flame-turbulence interaction of this DNS database may be found in [27, 28]. The present simulation time is short, but remains comparable to several studies [3, 8–10, 14, 34–37] which have contributed significantly to the fundamental understanding and modelling of turbulent premixed combustion in the past. The DNS data was explicitly filtered according to the integral $\overline{Q(\vec{x})} = \int Q(\vec{x} - \vec{r})G(\vec{r})d\vec{r}$ using a Gaussian kernel given by the expression $G(\vec{r}) = (6/\pi\Delta^2)^{3/2}\exp(-6\vec{r}\cdot\vec{r}/\Delta^2)$. The results will be presented for $\Delta$ ranging from $\Delta = 4\Delta_m \approx 0.4\delta_{\text{th}}$ to $\Delta = 24\Delta_m \approx 2.4\delta_{\text{th}}$, where $\Delta_m$ is the DNS grid spacing ($\Delta_m \approx 0.1\delta_{\text{th}}$). These filter sizes are comparable to the range of $\Delta$ used in *a priori* DNS analysis in several previous studies [3, 8–10, 14], and span a useful range of length scales from $\Delta$ comparable to $0.4\delta_{\text{th}} \approx 0.8\delta_z$, where the flame is partially resolved, up to $2.4\delta_{\text{th}} \approx 4.8\delta_z$, where the flame becomes fully unresolved and $\Delta$ is comparable to the integral length scale. For these filter widths, the underlying combustion process ranges from the "laminar flamelets-*G* DNS" [38] combustion regime (for $\Delta = 0.4\delta_{\text{th}} \approx 0.8\delta_z$) to well within the TRZ regime (for $\Delta \geq 0.5\delta_{\text{th}} \approx \delta_z$) on the regime diagrams by Pitsch and Duchamp de Lageneste [38] and Düsing et al. [39]. However, these regime diagrams have been proposed based on scaling arguments for unity Lewis number flames and the likely effects of nonunity Lewis number on these regime diagrams have yet to be ascertained. This topic is the subject of a separate investigation and will not be taken up in this paper.

## 4. Results and Discussion

*4.1. Effects of Le on D and $\eta_i$.* The power law expression (2b) for $\Sigma_{\text{gen}}$ may be rewritten as:

$$\log\left[\frac{\langle\Sigma_{\text{gen}}\rangle}{\langle|\nabla\bar{c}|\rangle}\right] = (D-2)\log\Delta - (D-2)\log(\eta_i), \quad (10)$$

where the angled brackets indicate a volume-averaging operation. The variation of $\langle\Sigma_{\text{gen}}\rangle/\langle|\nabla\bar{c}|\rangle$ with the ratio $(\Delta/\delta_z)$ is shown in Figure 1 on a log-log plot for all the different Lewis number cases. The quantity $\langle\Sigma_{\text{gen}}\rangle$ denotes the total flame surface area which remains independent of filter size $\Delta$. By contrast, the quantity $\langle|\nabla\bar{c}|\rangle$ denotes the resolved portion of the flame wrinkling, which decreases with increasing $\Delta$. As a result, $\log[\langle\Sigma_{\text{gen}}\rangle/\langle|\nabla\bar{c}|\rangle]$ increases with increasing $\Delta$. The variation of $\log[\langle\Sigma_{\text{gen}}\rangle/\langle|\nabla\bar{c}|\rangle]$ with $\log(\Delta/\delta_z)$ is linear when $\Delta \gg \delta_z$ but becomes nonlinear for $\Delta \ll \delta_z$. The best-fit straight line representing the greatest slope of the linear variation has been used to obtain values of $D$ and $\eta_i$. It has been found that $\eta_i/\delta_z$ remains independent of Le, and for all cases $\eta_i$ remains on the order of thermal flame thickness $\delta_{\text{th}}$ (i.e., $\eta_i/\delta_{\text{th}} \approx 1.0$), which is about twice the Zel'dovich flame thickness $\delta_z$ for the present thermochemistry (i.e., $\eta_i = 1.79\delta_z \approx \delta_{\text{th}}$). The scaling of the inner cut-off scale $\eta_i$ with $\delta_z$ is consistent with previous DNS [9] and experimental [7, 18] findings. Figure 1 shows that the slope of the linear region decreases with increasing Lewis number (i.e., in moving from case a to case e), which suggests that the fractal dimension $D$ decreases with increasing Le.

Contours of reaction progress variable $c$ in the $x_1 - x_2$ midplane are shown in Figure 2 for all cases and show that the extent of flame wrinkling is significantly greater at lower Lewis number. The rate of flame area generation increases with decreasing Le, and this behaviour is particularly noticeable for the cases with Le = 0.34 and Le = 0.6 because of the occurrence of thermo-diffusive instabilities [21, 24–28]. This can be substantiated from values of the ratio of turbulent to laminar flame surface area $A_T/A_L$ obtained by volume integration of $|\nabla c|$ (i.e., $A = \int_{\vartheta}|\nabla c|d\vartheta$). This produces the values $A_T/A_L$ =3.93, 2.66, 2.11, 1.84, and 1.76 for the cases with Le = 0.34, 0.6, 0.8, 1.0, and 1.2, respectively, at the time when statistics were extracted. The experimental findings of North and Santavicca [19] suggested that $D$ increases with increasing $u'/S_L \sim \text{Re}_t^{1/4}\text{Ka}^{1/2}$, which indicates that $D$ is expected to have a dependence on both $\text{Re}_t$ and Ka. Moreover, the analysis of Kerstein [20] suggested that $D$ is expected to assume an asymptotic value of 7/3 for large values of $\text{Re}_t$ and Ka. The present findings indicate that Le also has an influence on $D$ in addition to $\text{Re}_t$ and Ka, and that $D$ can assume values greater than 7/3 for flames with Le $\ll$ 1.0 (see Figure 1). The Karlovitz number Ka dependence of $D$ for unity Lewis number flames has been analysed in detail by Chakraborty and Klein [9] and they parameterised $D$ as: $D = 2 + (1/3)\,\text{erf}(2\text{Ka})$, which does not account for the effects of $\text{Re}_t$ and Le. The parameterisation proposed by Chakraborty and Klein [9] has been extended here by accounting for the effects of Karlovitz number, turbulent Reynolds number, and

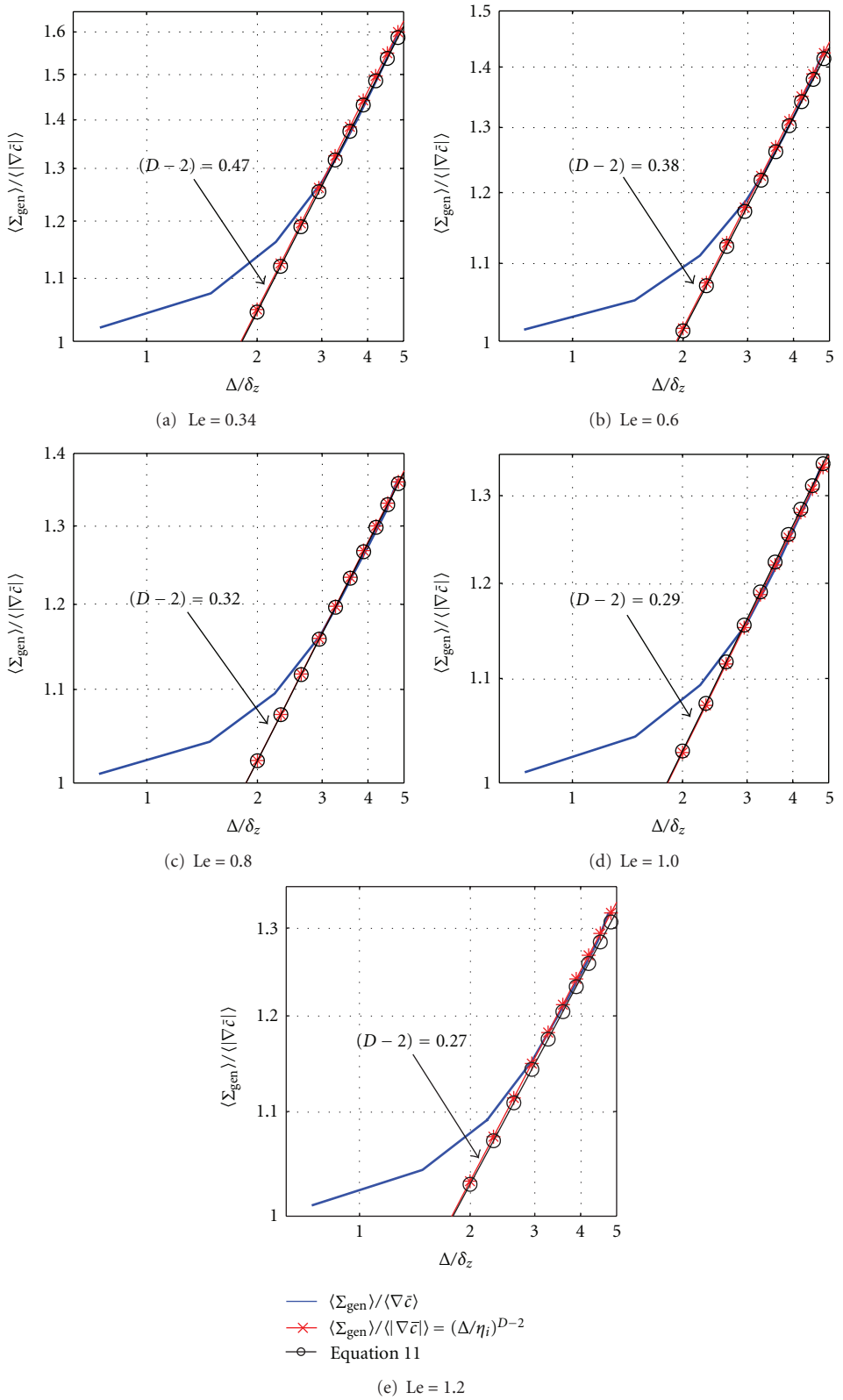


(a) Le = 0.34 (b) Le = 0.6 (c) Le = 0.8 (d) Le = 1.0 (e) Le = 1.2

FIGURE 1: Variation of $\langle\Sigma_{gen}\rangle/\langle\nabla\tilde{c}\rangle$ with $\Delta/\delta_z$ on a log-log plot for (a–e) cases A–E. Prediction of $\langle\Sigma_{gen}\rangle/\langle|\nabla\tilde{c}|\rangle = (\Delta/\eta_i)^{D-2}$ with $\eta_i$ obtained from DNS and $(D-2)$ according to (11) is also shown.

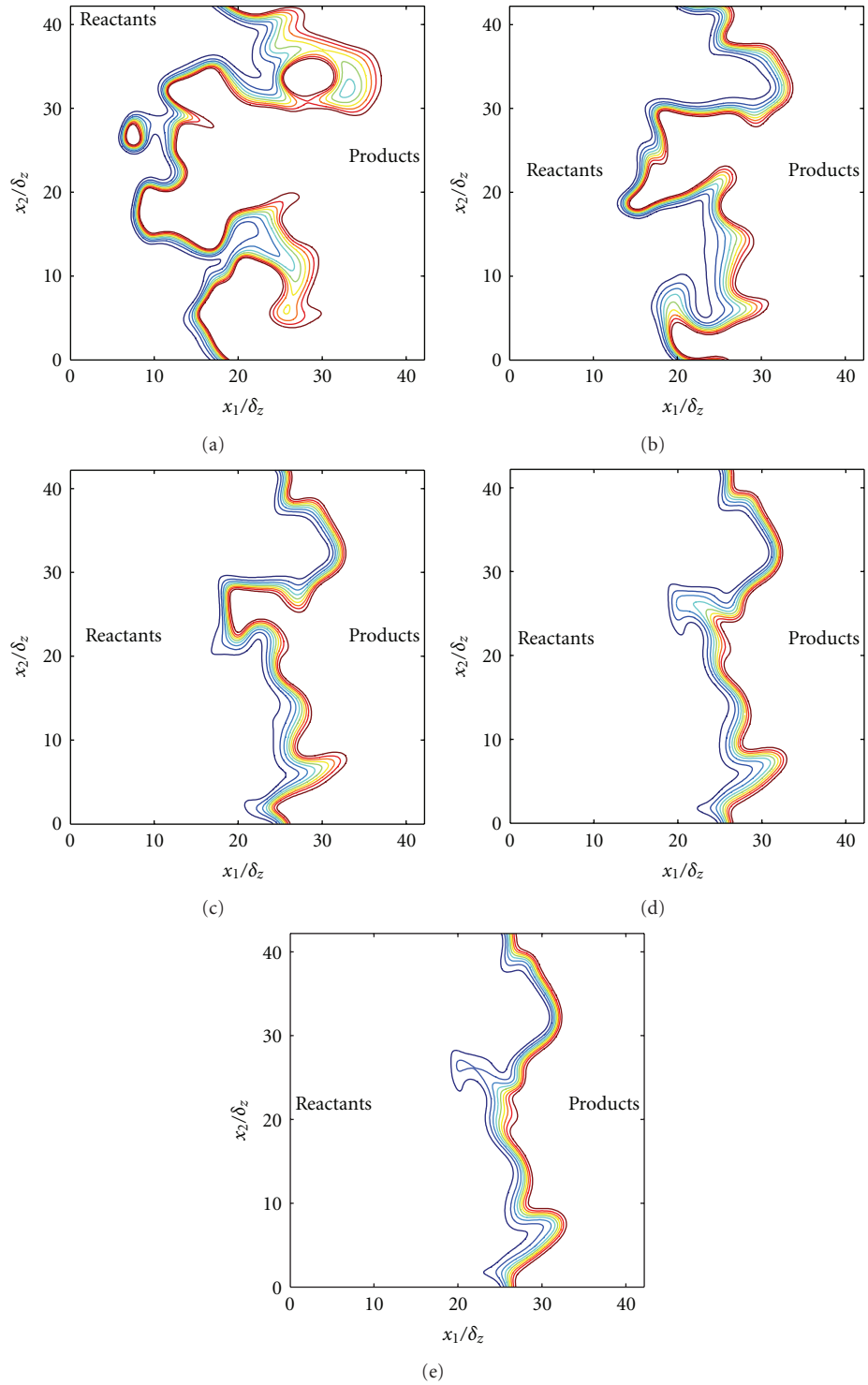


FIGURE 2: Contours of $c$ in the $x_1 - x_2$ midplane at time $t = \delta_{\text{th}}/S_L$ for (a–e) cases A–E.

global Lewis number (i.e., Ka, $\text{Re}_t$, and Le) according to the following:

$$D = 2 + \frac{1}{3}\,\text{erf}(3.0\text{Ka})\left[1 - \exp\left(-0.1\left(\frac{\text{Re}_t}{A_m}\right)^{1.6}\right)\right]\text{Le}^{-0.45}, \tag{11}$$

where $A_m \approx 7.5$ is a model parameter. Further details on the basis of this parameterisation are given in Appendix A.

The prediction of $\langle\Sigma_{\text{gen}}\rangle/\langle|\nabla\bar{c}|\rangle = (\Delta/\eta_i)^{D-2}$ with $\eta_i$ obtained from DNS and $D$ obtained from (11) is also shown in Figure 1, which indicates that (11) satisfactorily captures the best-fit straight line corresponding to the

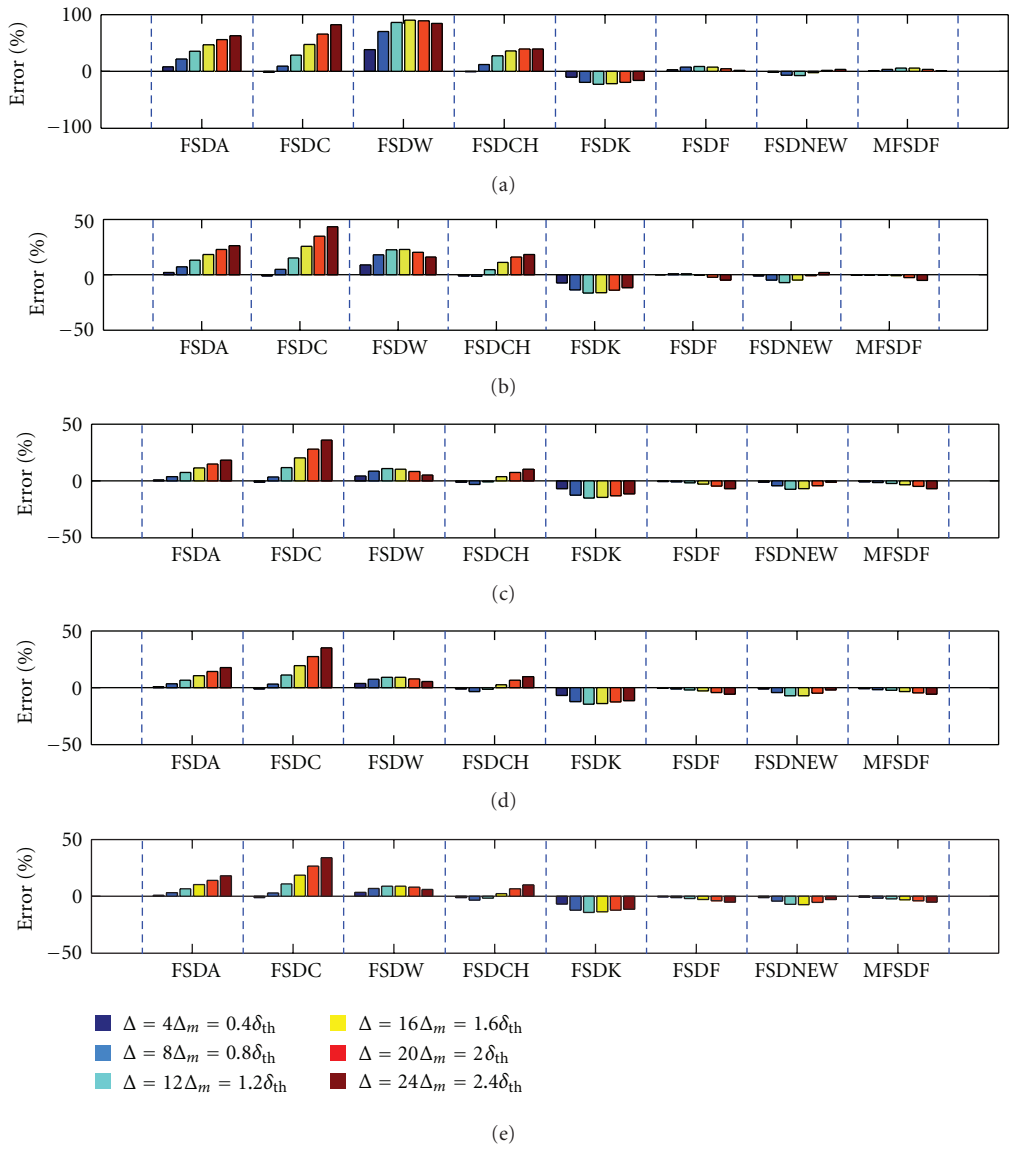


FIGURE 3: Percentage error (13) of the model prediction from $\langle \Sigma_{\text{gen}} \rangle$ obtained from DNS for LES filter widths $\Delta = 4\Delta_m = 0.4\delta_{\text{th}}$; $\Delta = 8\Delta_m = 0.8\delta_{\text{th}}$; $\Delta = 12\Delta_m = 1.2\delta_{\text{th}}$; $\Delta = 16\Delta_m = 1.6\delta_{\text{th}}$; $\Delta = 20\Delta_m = 2.0\delta_{\text{th}}$; $\Delta = 24\Delta_m = 2.4\delta_{\text{th}}$ for (a–e) cases A–E.

power law. It is worth noting that $\text{Re}_t$ and Ka in (11) were evaluated for this purpose based on $u'/S_L$ and $l/\delta_{\text{th}}$ in the unburned reactants. However, in actual LES simulations, $D$ needs to be evaluated based on local velocity and length scale ratios (i.e., $u'_\Delta/S_L$ and $\Delta/\delta_z$). Here $u'_\Delta$ is estimated from the subgrid turbulent kinetic energy as $u'_\Delta = \sqrt{2\tilde{k}_\Delta/3}$ following previous studies [12, 15, 16]. The local Karlovitz number $\text{Ka}_\Delta$ can be evaluated as $\text{Ka}_\Delta = C_{\text{Ka}}(\sqrt{k_\Delta}/S_L)^{3/2}(\delta_z/\Delta)^{1/2}$, where $C_{\text{Ka}}$ is a model parameter. Similarly, the local turbulent Reynolds number $\text{Re}_{t\Delta}$ can be evaluated using $\text{Re}_{t\Delta} = C_{\text{Re}}(\rho_0 u'_\Delta \Delta/\mu_0)$. The choice of model constants $C_{\text{Ka}} = 6.6$ and $C_{\text{Re}} = 4.0$ ensures an accurate prediction of $D$ for $\Delta \geq \eta_i$ and yields the value of $D$ obtained based on the global quantities according to (11).

Based on the observed behaviour of $D$ and $\eta_i$, a power-law expression for $\Sigma_{\text{gen}}$ is proposed here (model FSDNEW):

$$\Sigma_{\text{gen}} = |\nabla \bar{c}| \left[ (1 - f) + f \left( \frac{\Delta}{\eta_i} \right)^{D-2} \right], \tag{12}$$

where $f$ is a bridging function which increases monotonically from zero for small $\Delta$ (i.e., $\Delta/\delta_{\text{th}} \to 0$ or $\Delta \ll \delta_{\text{th}}$) to unity for large $\Delta$ (i.e., $\Delta \gg \eta_i$ or $\Delta \gg \delta_{\text{th}}$). Equation (12) ensures that $\Sigma_{\text{gen}}$ approaches $|\nabla \bar{c}|(\Delta/\eta_i)^{D-2}$ for large $\Delta$ and at the same time $\Sigma_{\text{gen}}$ approaches $|\nabla \bar{c}|$ (i.e., $\lim_{\Delta \to 0} \Sigma_{\text{gen}} = \lim_{\Delta \to 0} |\nabla \bar{c}| = |\nabla c|$) for small $\Delta$. It has been found that $\Sigma_{\text{gen}} \approx |\nabla \bar{c}|$ provides better agreement with $\Sigma_{\text{gen}}$ obtained from DNS data for $\Delta \leq 0.8\eta_i$, whereas the power-law $\Sigma_{\text{gen}} = |\nabla \bar{c}|(\Delta/\eta_i)^{D-2}$ starts to predict $\Sigma_{\text{gen}}$ more accurately for

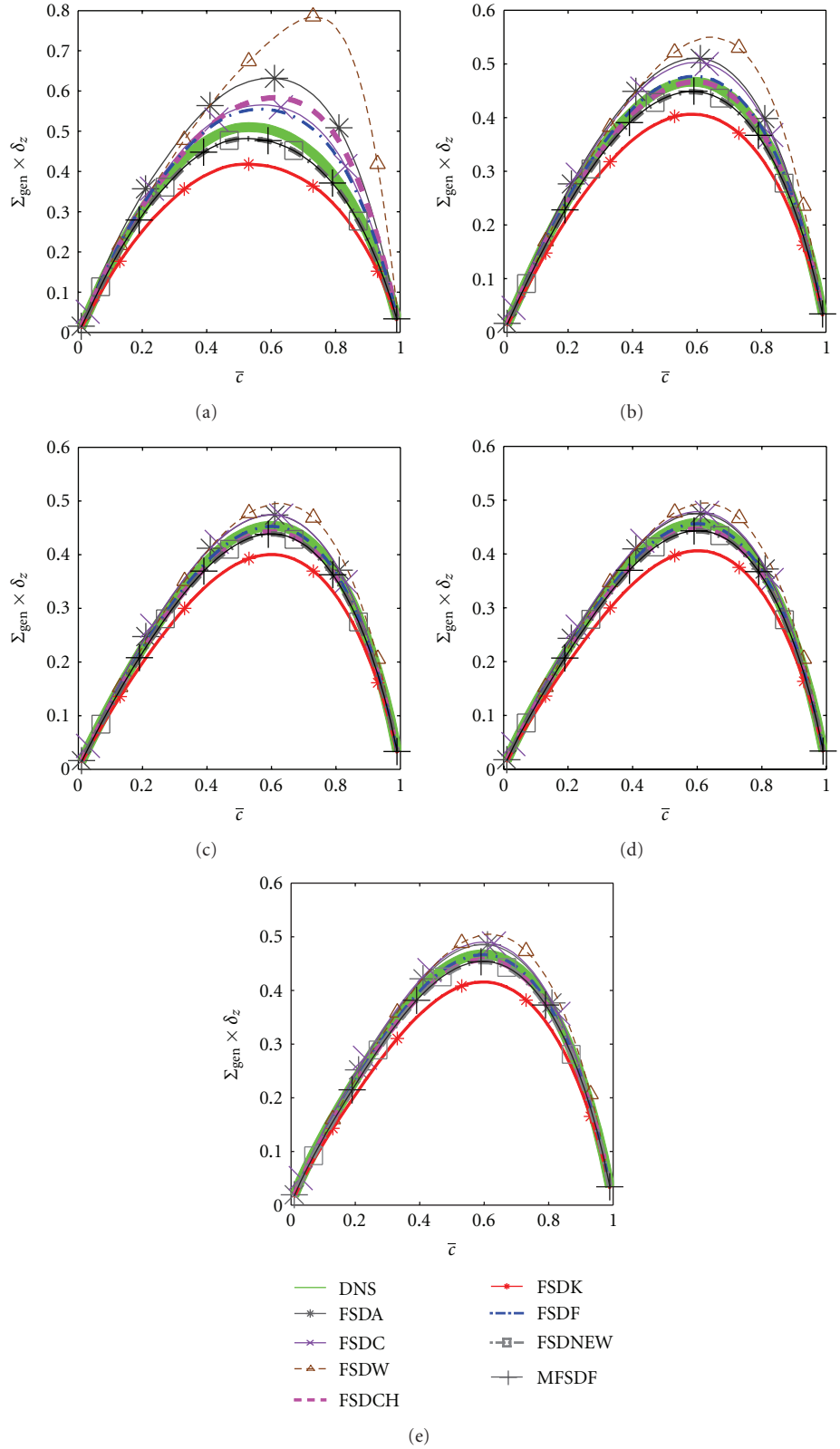


FIGURE 4: Variation of mean values of $\Sigma_{gen} \times \delta_z$ conditional on $\bar{c}$ across the flame brush for $\Delta = 8\Delta_m = 0.8\delta_{th}$ according to DNS, FSDA, FSDC, FSDW, FSDCH, FSDK, FSDF, FSDNEW, and MFSDF predictions for (a–e) cases A–E.

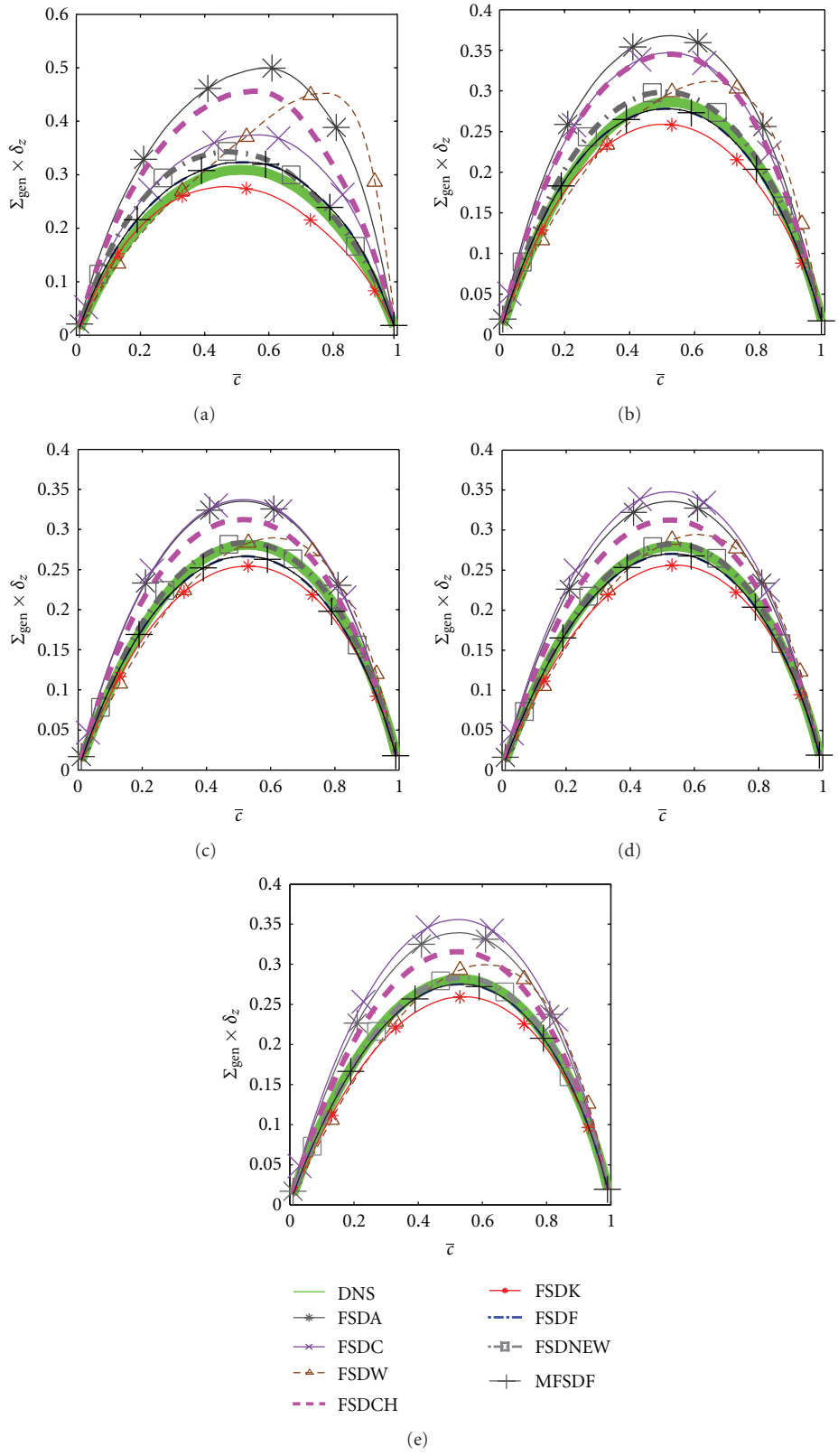


FIGURE 5: Variation of mean values of $\Sigma_{gen} \times \delta_z$ conditional on $\bar{c}$ across the flame brush for $\Delta = 24\Delta_m = 2.4\delta_{th}$ according to DNS, FSDA, FSDC, FSDW, FSDCH, FSDK, FSDF, FSDNEW, and MFSDF predictions for (a–e) cases A–E.

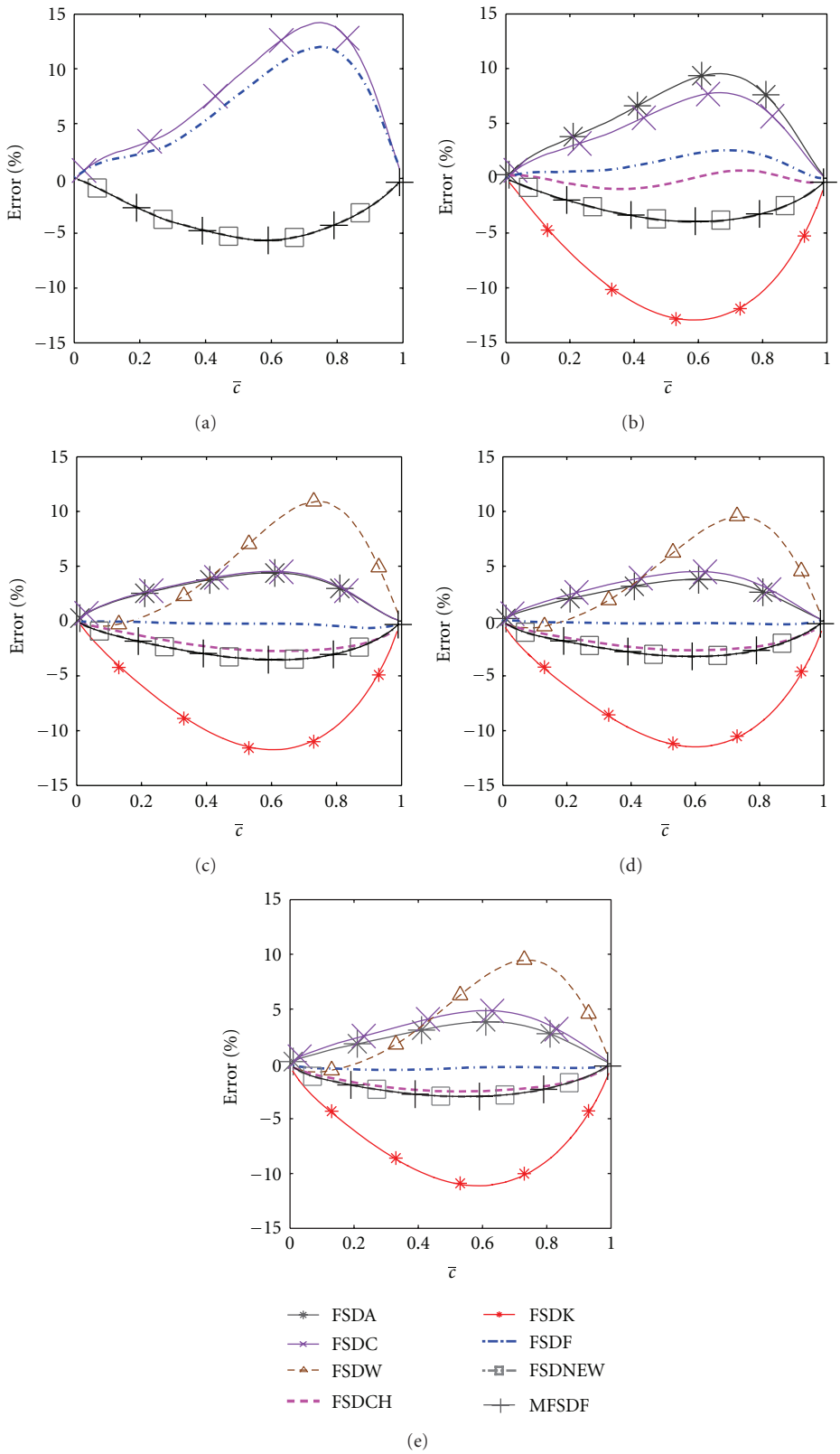


FIGURE 6: Variation of percentage error (17) on $\bar{c}$ across the flame brush for $\Delta = 8\Delta_m = 0.8\delta_{th}$ according to FSDA, FSDC, FSDW, FSDCH, FSDK, FSDF, FSDNEW, and MFSDF predictions for (a–e) cases A–E.

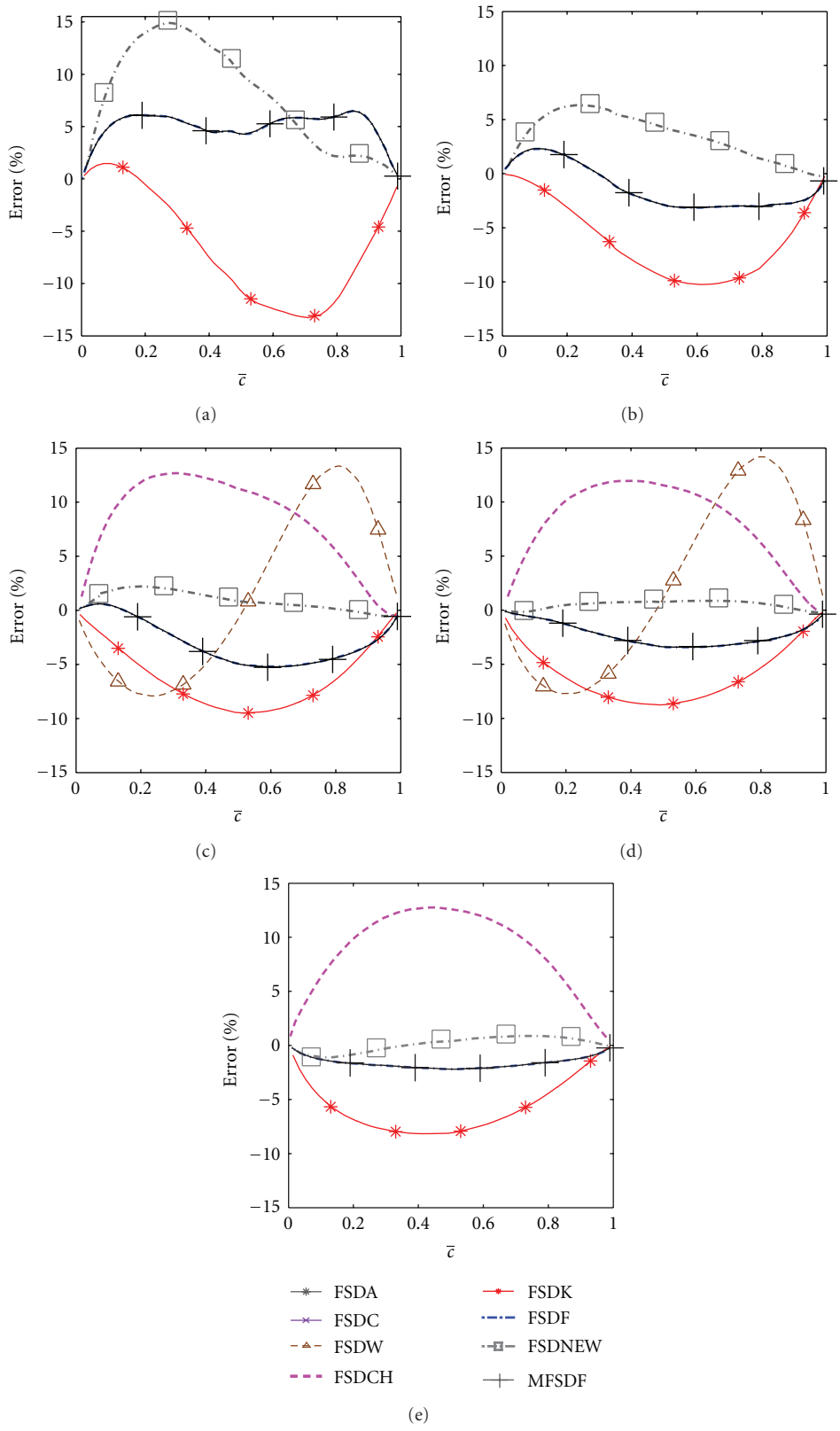


FIGURE 7: Variation of percentage error (17) on $\overline{c}$ across the flame brush for $\Delta = 24\Delta_m = 2.4\delta_{\text{th}}$ according to FSDA, FSDC, FSDW, FSDCH, FSDK, FSDF, FSDNEW, and MFSDF predictions for (a–e) cases A–E.

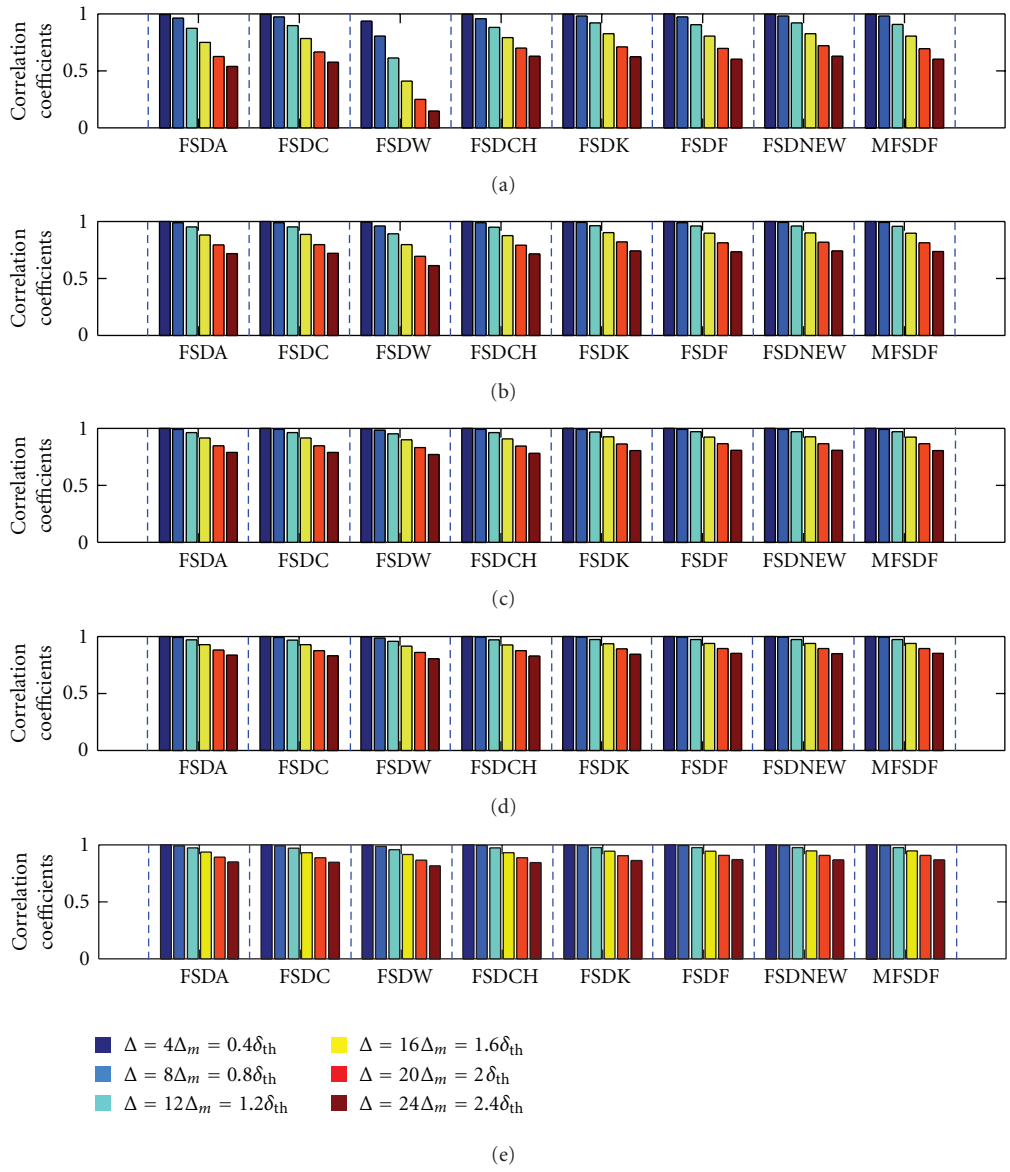


FIGURE 8: Correlation coefficients between the modelled and the actual values of $\Sigma_{gen}$ in the $\bar{c}$ range $0.1 \le \bar{c} \le 0.9$ for filter widths $\Delta = 4\Delta_m = 0.4\delta_{th}$; $\Delta = 8\Delta_m = 0.8\delta_{th}$; $\Delta = 12\Delta_m = 1.2\delta_{th}$; $\Delta = 16\Delta_m = 1.6\delta_{th}$; $\Delta = 20\Delta_m = 2.0\delta_{th}$; $\Delta = 24\Delta_m = 2.4\delta_{th}$ for (a–e) cases A–E.

$\Delta \ge 1.2\eta_i$ (see Figure 1). Based on this observation, the bridging function $f$ is taken to be $f = 1/[1+\exp\{-60(\Delta/\eta_i - 1.0)\}]$, which ensures a smooth transition between $0.8\eta_i < \Delta < 1.2\eta_i$. As $\eta_i$ is found to scale with $\delta_z$ (i.e., $\eta_i \approx 1.79\delta_z \approx \delta_{th}$ according to the present thermochemistry), $\eta_i$ in (12) is taken to be the thermal flame thickness $\delta_{th}$.

The performance of the various algebraic models for $\Sigma_{gen}$ will be assessed next, using the model requirements stated earlier.

*4.2. Performance of Models for the Volume-Averaged FSD* $\langle\Sigma_{gen}\rangle$. The inaccuracy in the model predictions of $\langle\Sigma_{gen}\rangle$ can be characterised using a percentage error (PE):

$$\mathrm{PE} = \frac{\left\langle\Sigma_{gen}\right\rangle_{model} - \left\langle\Sigma_{gen}\right\rangle}{\left\langle\Sigma_{gen}\right\rangle} \times 100, \qquad (13)$$

where $\langle\Sigma_{gen}\rangle_{model}$ is the volume-averaged value of the model prediction of $\langle\Sigma_{gen}\rangle$. Results for the PE for a range of filter size $\Delta$ are shown Figure 3. These demonstrate that the models denoted by FSDA (see (3a) and (3b)) and FSDC (see (5)) overpredict $\langle\Sigma_{gen}\rangle$ for all the Lewis number cases, and that the level of overprediction increases with increasing $\Delta$. The FSDW model (see (4)) also overpredicts $\langle\Sigma_{gen}\rangle$, although the level of overprediction decreases for $\Delta \gg \delta_{th}$, especially for cases with Le $\ge$ 0.6 (i.e., cases B–E). The FSDC model has greater PE than both the FSDA and FSDW models for all $\Delta$ in the same cases. However, the FSDW model has the highest PE relative to both the FSDA and FSDC models for all $\Delta$ in the Le = 0.34 case.

The FSDCH (6), FSDA, and FSDC models provide accurate predictions of $\langle\Sigma_{gen}\rangle$ at small values of $\Delta$ (i.e., $\Delta \ll \delta_z$) but they overpredict $\langle\Sigma_{gen}\rangle$ for large values of $\Delta$ (i.e.,

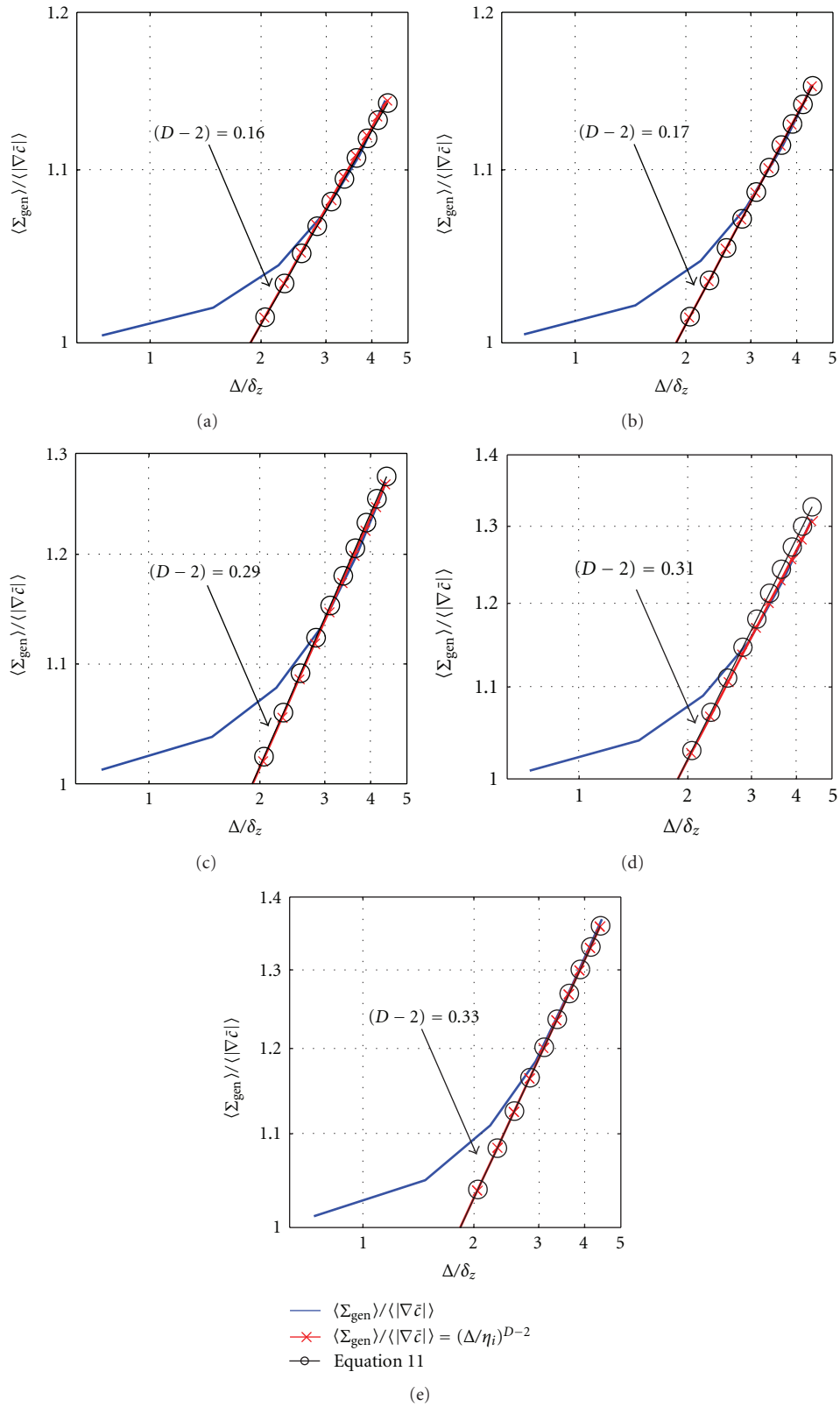


FIGURE 9: Variation of $\langle \Sigma_{gen} \rangle / \langle |\nabla \bar{c}| \rangle$ with $\Delta/\delta_z$ on a log-log plot for (a–e) cases A1–E1. The prediction of $\langle \Sigma_{gen} \rangle / \langle |\nabla \bar{c}| \rangle = (\Delta/\eta_i)^{D-2}$ with $\eta_i$ obtained from DNS and $(D-2)$ according to (11) is also shown.

$\Delta \gg \delta_z$). The FSDF model (9) predicts accurately for small $\Delta$, and marginally underpredicts for larger $\Delta$, for cases with Le $\geq$ 0.6. However, the FSDF model remains better than the FSDA, FSDC, FSDCH, and FSDW models. The FSDNEW model (12) provides an accurate prediction of $\langle\Sigma_{\text{gen}}\rangle$ for all filter sizes because this model is designed to do so for all values of Le. The PE for the FSDCH model remains small for cases with Le $\approx$ 1.0 (i.e., cases C–E), although the FSDCH model overpredicts $\langle\Sigma_{\text{gen}}\rangle$ for $\Delta \gg \delta_{\text{th}}$ for cases with Le $\ll$ 1 (i.e., cases A and B). The FSDK model (see (8)) underpredicts the value of $\langle\Sigma_{\text{gen}}\rangle$ for all $\Delta$ for all cases. However, the level of underprediction of the FSDK model decreases for larger $\Delta$.

The PEs for the FSDF and FSDNEW models remain negligible in comparison to the PEs for all the other models. Note that $\Sigma_{\text{gen}}$ should approach $|\nabla c|$ (i.e., $\lim_{u'_\Delta \to 0}\Sigma_{\text{gen}} = \lim_{u'_\Delta \to 0}\overline{|\nabla c|} = |\nabla c|$) when $u'_\Delta$ vanishes because the flow tends to be fully resolved (i.e., $\lim_{\Delta\to 0} u'_\Delta = 0$ and $\lim_{\Delta\to 0}\Sigma_{\text{gen}} = |\nabla c|$). Although the FSDF model performs well for all $\Delta$ for all the cases considered here, $\Sigma_{\text{gen}}$ does not tend to $|\nabla c|$ as $u'_\Delta$ approaches zero, but instead predicts a finite value close to zero. This limitation of the FSDF model can be avoided using a modified form of (8) (MSFDF model):

$$\Sigma_{\text{gen}} = |\nabla \bar{c}|\left[(1-f) + f\left(\Gamma\frac{u'_\Delta}{S_L}\right)^{D-2}\right], \tag{14}$$

where $f = 1/[1+\exp\{-60(\Delta/\delta_{\text{th}} - 1.0)\}]$ is a bridging function as before, the efficiency function $\Gamma$ is given by (3b) and $D = 2.05/(u'_\Delta/S_L + 1) + 2.35/(S_L/u'_\Delta + 1)$ [19]. Equation (14) ensures that $\Sigma_{\text{gen}}$ becomes exactly equal to $|\nabla c|$ when the flow is fully resolved (i.e., $\Delta \ll \eta_i$ or $\Delta \to 0$), where $u'_\Delta$ also vanishes (i.e., $\lim_{\Delta\to 0} u'_\Delta = 0$). Figure 3 shows that the modification given by (14) does not appreciably alter the performance of (8) while ensuring the correct asymptotic behaviour. Note that the parameterisation of $D$ and $\Gamma$ according to [19] and (3b), respectively, is essential for the satisfactory performance of the FSDF model. Using (13), for $D$ in the FSDF model is found to lead to a deterioration in its performance. Similarly, using $D$ as given by [19] in (12) worsens the performance of the FSDNEW model.

The FSDK model is based on the power-law $\Xi = (\eta_0/\eta_i)^{D-2}$ which is strictly valid only for filter sizes $\Delta$ which are sufficiently greater than $\eta_i$ (i.e., $\Delta \gg \eta_i$), as can be seen from Figure 1. Hence, the predictive capability of the FSDK model improves when $\Delta > \eta_i$ (see Figure 3). However, the FSDK model underpredicts $\langle\Sigma_{\text{gen}}\rangle$ because the inner cut-off scale is taken to be $3\delta_z$ in this model whereas $\eta_i \approx 1.79\delta_z$ for all the cases considered here. An accurate estimation of $\eta_i$ in the framework of the FSDK model results in comparable performance to the FSDNEW model for large $\Delta$ (i.e., $\Delta \gg \eta_i$). Moreover, $\Sigma_{\text{gen}}$ vanishes when $\Delta \to 0$ according to the FSDK model, whereas $\Sigma_{\text{gen}}$ should approach $|\nabla c|$ when $\Delta \to 0$ (i.e. $\lim_{u'_\Delta\to 0}\Sigma_{\text{gen}} = \lim_{u'_\Delta\to 0}\overline{|\nabla c|} = |\nabla c|$). This limitation can be avoided by modifying the FSDK model in the same manner as shown in (14) for the FSDF model (not shown here for conciseness).

The stretch-rate $\mathrm{K} = (1/\delta A)d(\delta A)/dt = a_T + S_d\nabla\cdot\vec{N}$ represents the fractional rate of change of flame surface area $A$ [1], where $S_d = Dc/Dt/|\nabla c|$ is the displacement speed, $\vec{N} = -\nabla c/|\nabla c|$ is the local flame normal vector and $a_T = (\delta_{ij} - N_iN_j)\partial u_i/\partial x_j$ is the tangential strain rate. It is possible to decompose $S_d$ into the reaction, normal diffusion and tangential diffusion components (i.e., $S_r, S_n$, and $S_t$) [8–10, 40, 41]:

$$S_r = \frac{\dot{w}}{\rho|\nabla c|}, \qquad S_n = \frac{\vec{N}\cdot\nabla\left(\rho D_c\vec{N}\nabla c\right)}{\rho|\nabla c|}, \qquad S_t = -D_c\nabla\cdot\vec{N}. \tag{15}$$

It has been shown in several previous studies [5, 6, 8, 10, 25] that $\overline{(a_T)}_s$ remains positive throughout the flame brush and thus acts to generate flame surface area, whereas the contribution of curvature to stretch $\overline{(S_d\nabla\cdot\vec{N})}_s = \overline{[(S_r+S_n)\nabla\cdot\vec{N}]}_s - \overline{[D_c(\nabla\cdot N)^2]}_s$ is primarily responsible for flame surface area destruction. The equilibrium of flame surface area generation and destruction yields $\overline{(\mathrm{K})}_s = 0$, which gives rise to [9]:

$$\overline{(a_T)}_s = -\overline{\left[(S_r+S_n)\nabla\cdot\vec{N}\right]}_s + \overline{\left[D_c\left(\nabla\cdot\vec{N}\right)^2\right]}_s. \tag{16}$$

The stretch rate induced by $-\overline{[D_c(\nabla\cdot\vec{N})^2]}_s$ becomes the leading order sink term in the thin reaction zones regime [8–10, 42]. However, most algebraic models (e.g., FSDA, FSDC, FSDCH, and FSDW) were proposed in the CF regime based on the equilibrium of the stretch rates induced by $\overline{[(S_r+S_n)\nabla\cdot\vec{N}]}_s$ and $\overline{(a_T)}_s$, and the flame surface area destruction due to $-\overline{[D_c(\nabla\cdot\vec{N})^2]}_s$ was ignored [4, 12–14]. As a result, these models underestimate the flame surface area destruction rate in the thin reaction zones regime, which leads to overprediction of $\langle\Sigma_{\text{gen}}\rangle$ for the FSDA, FSDC, FSDCH, and FSDW models.

The disagreement between the FSDF model prediction and DNS data originates principally due to the inaccuracy in estimating $\Gamma$ and $D$, while the difference between the FSDK prediction and DNS data arises from inaccurate estimation of $\eta_i$. Hence a more accurate estimation of $\Gamma$, $D$, and $\eta_i$ will result in better performance of both the FSDF and FSDK models.

*4.3. Performance of Models for the Variation of $\Sigma_{gen}$.* It is important to assess the models based on their ability to capture the correct variation of $\Sigma_{\text{gen}}$ with $\bar{c}$ across the flame brush. The variation of mean $\Sigma_{\text{gen}}$ conditionally averaged on $\bar{c}$ is shown in Figure 4 for $\Delta = 8\Delta_m = 0.8\delta_{\text{th}}$ and Figure 5 for $\Delta = 24\Delta_m = 2.4\delta_{\text{th}}$, respectively. These filter widths have been chosen since they correspond to $\Delta < \eta_i$ and $\Delta > \eta_i$ respectively. The following observations can be made from Figure 4 about the model predictions at $\Delta = 8\Delta_m = 0.8\delta_{\text{th}}$.

(i) The models FSDA, FSDC, FSDCH, FSDF, and FSDNEW tend to capture the variation of the conditional mean value of $\Sigma_{\text{gen}}$ with $\bar{c}$ obtained from DNS data. The prediction of the MFSDF model remains comparable to that of the FSDF model for $\Delta = 8\Delta_m = 0.8\delta_{\text{th}}$.

(ii) The FSDW model consistently overpredicts the conditional mean value of $\Sigma_{gen}$ for all cases. The FSDW model also predicts a skewed shape, which fails to capture the trend predicted by DNS.

(iii) The model FSDK underpredicts the conditional mean value of $\Sigma_{gen}$ in all cases. The physical explanations provided earlier for the underprediction of $\langle\Sigma_{gen}\rangle$ by the FSDK model is also responsible for the underprediction seen here.

A comparison between Figures 4 and 5 reveals that the predictions of the various algebraic FSD models exhibit greater spread for $\Delta = 24\Delta_m = 2.4\delta_{th}$ than in the case of $\Delta = 8\Delta_m = 0.8\delta_{th}$. The following observations can be made from Figure 5 about the model predictions at $\Delta = 24\Delta_m = 2.4\delta_{th}$.

(i) Similar to $\Delta = 8\Delta_m$, the FSDW model predicts a peak at $\bar{c} > 0.6$, whereas the peak value of conditionally averaged $\Sigma_{gen}$ from DNS occurs at $\bar{c} \approx 0.5$ for all the cases.

(ii) The models FSDW, FSDA, FSDC, and FSDCH tend to overpredict the conditionally averaged value of $\Sigma_{gen}$ and the level of the overprediction increases with decreasing Lewis number.

(iii) The models FSDF, FSDK, FSDNEW, and MFSDF tend to predict the conditionally averaged value of $\Sigma_{gen}$ satisfactorily throughout the flame brush.

(iv) The difference in the predictions of the models MFSDF, and FSDF seem to be very small for all the flames considered here.

The inaccuracy in the predictions of the mean value of $\Sigma_{gen}$ conditional on $\bar{c}$ can be characterised once again using a percentage error ($PE_2$):

$$PE_2 = \frac{\Sigma_{cond}^{MODEL} - \Sigma_{cond}^{DNS}}{\Sigma_{cond}^{max}} \times 100, \quad (17)$$

where $\Sigma_{cond}^{MODEL}$ and $\Sigma_{cond}^{DNS}$ are the mean values of $\Sigma_{gen}$ conditional on $\bar{c}$ as obtained from model prediction and DNS respectively, and $\Sigma_{cond}^{max}$ is the maximum value of conditionally averaged $\Sigma_{gen}$ obtained from DNS. The error in the model prediction according to (16) is shown in Figure 6 for filter size $\Delta = 8\Delta_m = 0.8\delta_{th}$ and in Figure 7 for filter size $\Delta = 24\Delta_m = 2.4\delta_{th}$. Note that the models predicting $PE_2$ outside a margin of ±15% have been discarded. In the case of Le = 0.34 (case A) the models FSDNEW, FSDF, MFSDF, and FSDC stay within the ±15% error limit for $\Delta = 8\Delta_m$ whereas only the models FSDF, MFSDF, FSDK and FSDNEW remain within the ±15% error limit for $\Delta = 24\Delta_m$. As Le increases to 0.6 (case B), the models FSDNEW, FSDCH, FSDF, MFSDF, FSDC, FSDA, and FSDK predict within the ±15% error margin and have been listed in terms of decreasing accuracy for $\Delta = 8\Delta_m$. For case B only the predictions of FSDNEW, FSDF, MFSDF and FSDK remain within the ±15% error margin for $\Delta = 24\Delta_m$. In the Le = 0.8 case (case C), the models FSDF, FSDNEW, MFSDF, FSDCH, FSDA, FSDC, FSDK and FSDW all provide predictions within ±15% for $\Delta = 8\Delta_m$, whereas the predictions of FSDNEW, FSDF, MFSDF, FSDCH, FSDK and FSDW remain within ±15% for $\Delta = 24\Delta_m$. For Le = 1.0 and 1.2 (cases D and E) the models FSDF, MFSDF, FSDNEW, FSDCH, FSDA, FSDC, FSDK and FSDW all predict within the ±15% error margin for $\Delta = 8\Delta_m$, while the models FSDF, MFSDF, FSDNEW, FSDK and FSDCH predict within ±15% for $\Delta = 24\Delta_m$. The model FSDW was found to predict within the ±15% error margin for $\Delta = 24\Delta_m$ in the Le = 1.0 flame but its prediction remains marginally beyond the ±15% error margin for $\Delta = 24\Delta_m$ for the Le = 1.2 flame considered here (The maximum magnitude of $PE_2$ for the FSDW model in the Le = 1.2 case is 15.2%, and the variation of $PE_2$ with $\bar{c}$ in this case is qualitatively similar to the Le = 1.0 case considered here).

Comparing the performance of the models at $\Delta = 8\Delta_m$ and $\Delta = 24\Delta_m$, it can be seen that FSDA, FSDCH and FSDC predict $\Sigma_{gen}$ satisfactorily at $\Delta = 8\Delta_m$ but the agreement with DNS deteriorates at $\Delta = 24\Delta_m$. By contrast, the FSDK prediction is closer to DNS data at $\Delta = 24\Delta_m$ than at $\Delta = 8\Delta_m$. The models FSDF, MFSDF, and FSDNEW fare well at both $\Delta = 8\Delta_m$ and $\Delta = 24\Delta_m$ for all the Lewis number values considered here. It is worth noting that the FSDNEW model was designed to predict the volume-averaged value of generalised FSD $\langle\Sigma_{gen}\rangle$, but judging from Figures 4–7, this model also performs satisfactorily with respect to predicting the correct variation of $\Sigma_{gen}$ across the flame brush.

The prediction of the model FSDK improves with increasing filter width Δ, unlike the other models, which is consistent with observations made in the context of Figure 3. The prediction of the FSDW model remains skewed towards the product side of the flame brush due to the $\tilde{c}$ dependence of Ξ (i.e., $\Xi = 1 + 1.24\tilde{c}\sqrt{u'_\Delta/S_L}\,\mathrm{Re}_\eta$) proposed in [12]. The FSDW, FSDA, FSDC, and FSDCH models underestimate the destruction rate of flame surface area in the thin reaction zones regime due to the underestimation of FSD destruction arising due to the curvature stretch contribution $-\overline{[D_c(\nabla\cdot\vec{N})^2]}_s$, which eventually leads to the overprediction of conditionally averaged value of $\Sigma_{gen}$.

*4.4. Performance of Models for the Local $\Sigma_{gen}$ Behaviour.* The FSD predicted by the models should have the correct resolved strain rate and curvature dependence in the context of LES and thus the correlation coefficient between the FSD obtained from DNS and from the model prediction should remain as close to unity as possible. The variation of the correlation coefficients between the model prediction and generalised FSD $\Sigma_{gen}$ obtained from DNS in the range of filtered reaction progress variable $0.1 \le \bar{c} \le 0.9$ are shown in Figure 8 for different filter widths. The regions corresponding to $0.1 < \bar{c}$ and $\bar{c} > 0.9$ have been ignored since the correlation coefficients have little physical significance in these regions due to the small values of $\Sigma_{gen}$ obtained from both DNS and model predictions. Figure 8 indicates that the correlation coefficients decrease with increasing Δ due to increased unresolved subgrid wrinkling, which makes the local variation of $\Sigma_{gen}$ different from $|\nabla\bar{c}|$. The extent of the deviation of the correlation coefficients from unity increases with decreasing Le for a given value of Δ. Figure 8

indicates that the models FSDA, FSDC, FSDCH, FSDF, MFSDF, FSDK, FSDNEW, and FSDW have comparable correlation coefficients, which deviate considerably from unity for large values of $\Delta$. This indicates that algebraic models may not be able to predict FSD such that its local strain rate and curvature dependencies can be appropriately captured, especially in the TRZ regime. Hence a transport equation for FSD might need to be solved to account for the local strain rate and curvature effects on $\Sigma_{\text{gen}}$ [5, 6, 8, 10, 11].

## 5. Conclusions

The performance of several wrinkling factor based LES algebraic models for $\Sigma_{\text{gen}}$ has been assessed for nonunity Lewis number flames in the TRZ regime based on a DNS database of freely propagating statistically planar turbulent premixed flames with Le ranging from 0.34 to 1.2. It has been found that the fractal dimension $D$ increases with decreasing Le, whereas Le does not have any significant influence on the value of the normalised inner cut-off scale $\eta_i/\delta_z$. For all Lewis number cases the inner cut-off scale is found to be equal to the thermal flame thickness (i.e., $\eta_i \approx \delta_{\text{th}}$). Based on the analysis of DNS data, a new parameterisation of $D$ is proposed, where the effects of Le are explicitly accounted for. This new parameterisation of $D$ has been used to propose a power-law based model for $\Sigma_{\text{gen}}$ to account for nonunity Lewis number effects. The performance of this new model has been assessed with respect to $\Sigma_{\text{gen}}$ obtained from DNS data alongside other existing models. The new model was found to be capable of predicting the behaviour of $\Sigma_{\text{gen}}$ in the TRZ regime with greater or comparable accuracy in comparison to the existing models for all values of Le considered here. However, the present study has been carried out for moderate values of turbulent Reynolds number $\text{Re}_t$ and the effects of detailed chemistry and transport are not accounted for. Thus, three-dimensional DNS with detailed chemistry will be necessary, together with experimental data, for a more comprehensive assessment of LES algebraic models for $\Sigma_{\text{gen}}$.

## Appendix

### A. Effects of $\text{Re}_t$ on Fractal Dimension $D$

The effects of $\text{Re}_t$ on $D$ have been analysed based on a simplified chemistry based DNS database [43, 44], in which the variation of $\text{Re}_t \sim \text{Da}^2\,\text{Ka}^2$ is brought about by modifying Da and Ka independently of each other. The initial values of $u'/S_L$ and $l/\delta_{\text{th}}$ for all the flames in this DNS database are shown in Table 1(a) along with the values of heat release parameter $\tau = (T_{\text{ad}} - T_0)/T_0$, Damköhler number $\text{Da} = lS_L/u'\delta_{\text{th}}$, Karlovitz number $\text{Ka} = (u'/S_L)^{3/2}(lS_L/\alpha_{T0})^{-1/2}$, and turbulent Reynolds number $\text{Re}_t = \rho_0 u' l/\mu_0$.

The variations of $\log(\langle\Sigma_{\text{gen}}\rangle/\langle|\nabla\bar{c}|\rangle)$ with $\log(\Delta/\delta_z)$ for cases A1–E1 are shown in Figure 9, which demonstrate that $D$ is greater for flames with higher $\text{Re}_t$, and that $D$ attains an asymptotic value of 7/3 for unity Lewis number flames with high values of $\text{Re}_t$ (e.g., cases D1 and E1). The prediction of $\langle\Sigma_{\text{gen}}\rangle/\langle|\nabla\bar{c}|\rangle = (\Delta/\eta_i)^{D-2}$ with $\eta_i$ obtained from DNS and $D$ obtained from (11) is also shown in Figure 9, which indicates that (11) satisfactorily captures the slope of the best-fit straight line.

## Acknowledgment

The authors are grateful to EPSRC, UK, for financial assistance.

## References

[1] S. M. Candel and T. J. Poinsot, "Flame stretch and the balance equation for the flame area," *Combustion Science and Technology*, vol. 70, no. 1–3, pp. 1–15, 1990.

[2] R. S. Cant, S. B. Pope, and K. N. C. Bray, "Modelling of flamelet surface-to-volume ratio in turbulent premixed combustion," *Proceedings of the Combustion Institute*, vol. 23, no. 1, pp. 809–815, 1991.

[3] M. Boger, D. Veynante, H. Boughanem, and A. Trouve, "Direct numerical simulation analysis of flame surface density concept for large eddy simulation of turbulent premixed combustion," *Proceedings of the Combustion Institute*, vol. 1, pp. 917–925, 1998.

[4] C. Angelberger, D. Veynante, F. Egolfopoulos, and T. Poinsot, "A flame surface density model for large eddy simulations of turbulent premixed flames," in *Proceedings of the Summer Program*, pp. 66–82, Center for Turbulence Research, Stanford, Calif, USA, 1998.

[5] E. R. Hawkes and R. S. Cant, "A flame surface density approach to large-eddy simulation of premixed turbulent combustion," *Proceedings of the Combustion Institute*, vol. 28, no. 1, pp. 51–58, 2000.

[6] E. R. Hawkes and R. S. Cant, "Implications of a flame surface density approach to large eddy simulation of premixed turbulent combustion," *Combustion and Flame*, vol. 126, no. 3, pp. 1617–1629, 2001.

[7] R. Knikker, D. Veynante, and C. Meneveau, "A dynamic flame surface density model for large eddy simulation of turbulent premixed combustion," *Physics of Fluids*, vol. 16, no. 11, pp. L91–L94, 2004.

[8] N. Chakraborty and R. S. Cant, "A priori analysis of the curvature and propagation terms of the flame surface density transport equation for large eddy simulation," *Physics of Fluids*, vol. 19, no. 10, Article ID 105101, 2007.

[9] N. Chakraborty and M. Klein, "A priori direct numerical simulation assessment of algebraic flame surface density models for turbulent premixed flames in the context of large eddy simulation," *Physics of Fluids*, vol. 20, no. 8, Article ID 085108, 2008.

[10] N. Chakraborty and R. S. Cant, "Direct numerical simulation analysis of the flame surface density transport equation in the context of large eddy simulation," in *32nd International Symposium on Combustion*, pp. 1445–1453, can, August 2008.

[11] F. E. Hernandez-Perez, F. T. C. Yuen, C. P. T. Groth, and O. L. Gulder, "LES of a laboratory-scale turbulent premixed Bunsen flame using FSD, PCM-FPI and thickened flame models," *Proceedings of the Combustion Institute*, vol. 33, pp. 1365–1371, 2011.

[12] H. G. Weller, G. Tabor, A. D. Gosman, and C. Fureby, "Application of a flame-wrinkling LES combustion model to a turbulent mixing layer," *Proceedings of the Combustion Institute*, vol. 1, pp. 899–907, 1998.

[13] O. Colin, F. Ducros, D. Veynante, and T. Poinsot, "A thickened flame model for large eddy simulations of turbulent premixed combustion," *Physics of Fluids*, vol. 12, no. 7, pp. 1843–1863, 2000.

[14] F. Charlette, C. Meneveau, and D. Veynante, "A power-law flame wrinkling model for LES of premixed turbulent combustion Part I: Non-dynamic formulation and initial tests," *Combustion and Flame*, vol. 131, no. 1-2, pp. 159–180, 2002.

[15] G. Tabor and H. G. Weller, "Large eddy simulation of premixed turbulent combustion using Ξ flame surface wrinkling model," *Flow, Turbulence and Combustion*, vol. 72, no. 1, pp. 1–28, 2004.

[16] C. Fureby, "A fractal flame-wrinkling large eddy simulation model for premixed turbulent combustion," *Proceedings of the Combustion Institute*, vol. 30, no. 1, pp. 593–601, 2005.

[17] N. Peters, *Turbulent Combustion*, Cambridge University Press, Cambridge, UK, 2000.

[18] W. L. Roberts, J. F. Driscoll, M. C. Drake, and L. P. Goss, "Images of the quenching of a flame by a vortex-To quantify regimes of turbulent combustion," *Combustion and Flame*, vol. 94, no. 1-2, pp. 58–69, 1993.

[19] G. L. North and D. A. Santavicca, "The fractal nature of turbulent premixed flames," *Combustion Science and Technology*, vol. 72, pp. 215–232, 1990.

[20] A. Kerstein, "Fractal dimension of turbulent premixed flames," *Combustion Science and Technology*, vol. 60, pp. 441–445, 1988.

[21] H. G. Im and J. H. Chen, "Preferential diffusion effects on the burning rate of interacting turbulent premixed hydrogen-air flames," *Combustion and Flame*, vol. 131, no. 3, pp. 246–258, 2002.

[22] E. R. Hawkes and J. H. Chen, "Direct numerical simulation of hydrogen-enriched lean premixed methane-air flames," *Combustion and Flame*, vol. 138, no. 3, pp. 242–258, 2004.

[23] N. Chakraborty, E. R. Hawkes, J. H. Chen, and R. S. Cant, "The effects of strain rate and curvature on surface density function transport in turbulent premixed $CH_4$-air and $H_2$-air flames: A comparative study," *Combustion and Flame*, vol. 154, no. 1-2, pp. 259–280, 2008.

[24] C. J. Rutland and A. Trouve, "Direct simulations of premixed turbulent flames with nonunity Lewis numbers," *Combustion and Flame*, vol. 94, no. 1-2, pp. 41–57, 1993.

[25] A. Trouvé and T. Poinsot, "Evolution equation for the flame surface density in turbulent premixed combustion," *Journal of Fluid Mechanics*, vol. 278, pp. 1–31, 1994.

[26] N. Chakraborty and R. S. Cant, "Influence of Lewis number on curvature effects in turbulent premixed flame propagation in the thin reaction zones regime," *Physics of Fluids*, vol. 17, no. 10, Article ID 105105, 2005.

[27] N. Chakraborty and R. S. Cant, "Effects of Lewis number on turbulent scalar transport and its modelling in turbulent premixed flames," *Combustion and Flame*, vol. 156, no. 7, pp. 1427–1444, 2009.

[28] N. Chakraborty and R. S. Cant, "Effects of Lewis number on flame surface density transport in turbulent premixed combustion," *Combustion and Flame*, vol. 158, no. 9, pp. 1768–1787, 2011.

[29] K. W. Jenkins and R. S. Cant, "DNS of turbulent flame kernels," in *Proceedings of the 2nd AFOSR Conference on DNS and LES*, Knight and Sakell, Eds., pp. 192–202, Rutgers University, Kluwer Academic Publishers, 1999.

[30] J. H. Chen, A. Choudhary, B. De Supinski et al., "Terascale direct numerical simulations of turbulent combustion using S3D," *Computational Science and Discovery*, vol. 2, no. 1, Article ID 015001, 2009.

[31] T. J. Poinsot, "Boundary conditions for direct simulations of compressible viscous flows," *Journal of Computational Physics*, vol. 101, no. 1, pp. 104–129, 1992.

[32] A. A. Wray, "Minimal storage time advancement schemes for spectral methods," Tech. Rep., NASA Ames Research Center, California, Calif, USA, 1990.

[33] R. S. Rogallo, "Numerical experiments in homogeneous turbulence," NASA Technical Memorandum 81315, NASA Ames Research Center, California, Calif, USA, 1981.

[34] N. Swaminathan and R. W. Grout, "Interaction of turbulence and scalar fields in premixed flames," *Physics of Fluids*, vol. 18, no. 4, Article ID 045102, 2006.

[35] W. R. Grout, "An age extended progress variable for conditioning reaction rates," *Physics of Fluids*, vol. 19, no. 10, Article ID 105107, 2007.

[36] I. Han and K. Y. Huh, "Roles of displacement speed on evolution of flame surface density for different turbulent intensities and Lewis numbers in turbulent premixed combustion," *Combustion and Flame*, vol. 152, no. 1-2, pp. 194–205, 2008.

[37] I. Han and K. Y. Huh, "Effects of the Karlovitz number on the evolution of the flame surface density in turbulent premixed flames," in *32nd International Symposium on Combustion*, pp. 1419–1425, can, August 2008.

[38] H. Pitsch and L. Duchamp de Lageneste, "Large-eddy simulation of premixed turbulent combustion using a level-set approach," in *Twenty-Ninth International Symposium on Combustion Hokkaido University Sapporo Japan*, pp. 2001–2008, jpn, July 2002.

[39] M. Düsing, A. Sadiki, and J. Janicka, "Towards a classification of models for the numerical simulation of premixed combustion based on a generalized regime diagram," *Combustion Theory and Modelling*, vol. 10, no. 1, pp. 105–132, 2006.

[40] N. Peters, P. Terhoeven, J. H. Chen, and T. Echekki, "Statistics of flame displacement speeds from computations of 2-D unsteady methane-air flames," *Proceedings of the Combustion Institute*, vol. 27, pp. 833–839, 1998.

[41] T. Echekki and J. H. Chen, "Analysis of the contribution of curvature to premixed flame propagation," *Combustion and Flame*, vol. 118, no. 1-2, pp. 308–311, 1999.

[42] E. R. Hawkes and J. H. Chen, "Evaluation of models for flame stretch due to curvature in the thin reaction zones regime," *Proceedings of the Combustion Institute*, vol. 30, no. 1, pp. 647–655, 2005.

[43] N. Chakraborty, M. Klein, and R. S. Cant, "Effects of turbulent Reynolds number on the displacement speed statistics in the thin reaction zones regime turbulent premixed combustion," *Journal of Combustion*, vol. 2011, Article ID 473679, 19 pages, 2011.

[44] N. Chakraborty, G. Hartung, M. Katragadda, and C. F. Kaminski, "Comparison of 2D and 3D density-weighted displacement speed statistics and implications for laser based measurements of flame displacement speed using direct numerical simulation data," *Combustion and Flame*, vol. 158, no. 7, pp. 1372–1390, 2011.